World Academy of Science, Engineering and Technology
International Journal of Energy and Power Engineering
Vol:11, No:5, 2017

Electrical and Thermal Characteristics of a Photovoltaic Solar Wall with Passive and Active Ventilation through a Room

Himanshu Dehra

***Abstract*—**An experimental study was conducted for ascertaining electrical and thermal characteristics of a pair of photovoltaic (PV) modules integrated with solar wall of an outdoor room. A pre-fabricated outdoor room was setup for conducting outdoor experiments on a PV solar wall with passive and active ventilation through the outdoor room. The selective operating conditions for glass coated PV modules were utilized for establishing their electrical and thermal characteristics. The PV solar wall was made up of glass coated PV modules, a ventilated air column, and an insulating layer of polystyrene filled plywood board. The measurements collected were currents, voltages, electric power, air velocities, temperatures, solar intensities, and thermal time constant. The results have demonstrated that: i) a PV solar wall installed on a wooden frame was of more heat generating capacity in comparison to a window glass or a standalone PV module; ii) generation of electric power was affected with operation of vertical PV solar wall; iii) electrical and thermal characteristics were not significantly affected by heat and thermal storage losses; and iv) combined heat and electricity generation were function of volume of thermal and electrical resistances developed across PV solar wall. Finally, a comparison of temperature plots of passive and active ventilation envisaged that fan pressure was necessary to avoid overheating of the PV solar wall. The active ventilation was necessary to avoid over-heating of the PV solar wall and to maintain adequate ventilation of room under mild climate conditions.

***Keywords*—**Photovoltaic solar wall, solar energy, passive ventilation, active ventilation.

I. Introduction

THE aim of this paper is to present experiments that were conducted on a PV solar wall for establishing their electrical and thermal characteristics under selective operating conditions. The salient feature of a pair of PV modules used in solar wall was the glass coating surrounding the semiconductor material of solar cells [1]-[4]. The manufacturing of glass coated PV modules was based on multi-crystalline solar cell technology. The operating conditions were selected for conducting various experiments on a PV solar wall. The indoor solar simulator tests were conducted for PV modules under standard operating conditions. The outdoor tests were conducted under available climatic conditions. The outdoor experiments were conducted for obtaining temperatures, air velocities, thermal time constants, heat capacity, and thermal storage capacity of a PV solar wall.

Himanshu Dehra is with Egis Group, Gurugram, Haryana 122003, India (phone: +91 9560052596; e-mail: anshu_dehra@hotmail.com).

Many studies on facade integrated PV system are focused on the model simulation of radiation and convection [5]. Kim and Kim [6] compared three different types of integrated PV-thermal system configurations. The study analyzed the system performance as well as the building performance. Various researchers [7], [8] have also conducted research on the energy performance and efficiency of actively air cooled PV modules integrated into facades. The PV modules used for experiments were having a glass coating of 3 mm attached on its exterior and interior sides [1]. The glass coating was attached to exterior and interior sides of PV modules in the form of glass sheets by a double-glass (PWX) manufacturing technology [2]. Each PV module was having 36 multi-crystalline solar cell units, with thin transparent gaps in between them [1], [2]. The glass coating on PV modules has improved the overall performance of PV modules in many ways; it has: i) protected semi-conductor material from weather deterioration; ii) absorbed ultra violet rays of solar energy and trap solar heat in glass coating, thus increasing the temperature of the surrounding environment; iii) reduced the reflection losses of sunlight rays reflected from PV module; iv) improved the aesthetic appearance of PV module; v) increased the thermal mass of PV module; and vi) enhanced the structural strength of PV module. The pictorial view of glass coated PV module used in experiments is illustrated in Fig. 1 [2]. The commercially available PV modules were having glass coating on their exterior and interior sides. The typical characteristics of glass coated PV module without frame were: dimensions of 993 mm by 453 mm and a thickness of 6.2 mm with glass coating [1], typical current of 2.8 A, typical voltage of 17 V, temperature coefficients of current and voltage were + 0.034 %/°C and -2.17 mV/°C/solar cell at standard test conditions [1], [2].

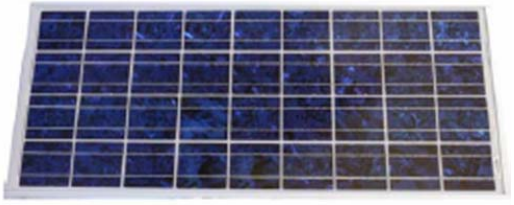

Fig. 1 Glass coated PV module used in experiments

II. Indoor Experiments

The indoor measurement tests were carried out on glass coated PV modules in an indoor simulation test facility of

CANMET Energy Technology Centre of Natural Resources, Varennes, Québec, Canada [1]. The schematic of indoor solar simulator used for establishing characteristics of glass coated PV modules is illustrated in Fig. 2.

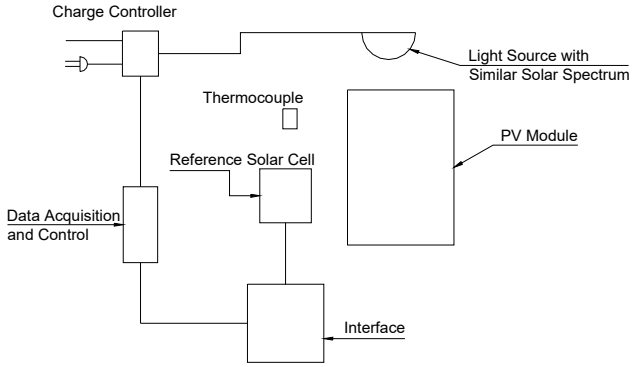

Fig. 2 Block diagram of an indoor solar simulator

The current-voltage and power-voltage characteristics of one of the PV modules are shown in Figs. 3 and 4 [1]. Table I has presented characteristics of a pair of PV modules established with an indoor solar simulator [1]. As presented in Table I, electrical conversion efficiency to the order of 8.9% was reported from indoor simulator tests.

TABLE I
CHARACTERISTICS OF GLASS COATED PV MODULES ESTABLISHED WITH AN INDOOR SOLAR SIMULATOR

PV Module	Solar Intensity (Wm^{-2})	Spectrum	Isc (A)	Voc (V)
PW30	1009.11	1.5 A.M. Class B	2.833	21.296
PW31	1007.58	1.5 A.M. Class B	2.829	21.352
PV Module	Vmax (V)	Pmax (Watts)	Fill factor	Efficiency (%)
PW30	16.198	42.157	0.6985	8.703
PW31	16.503	43.435	0.7188	8.981

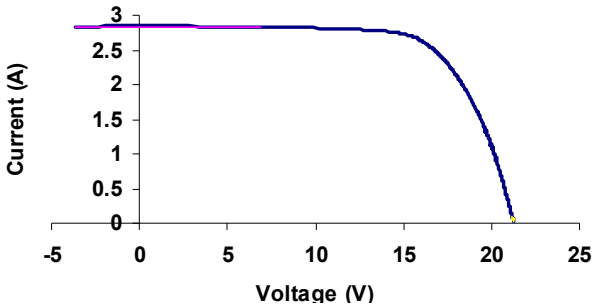

Fig. 3 Current-voltage characteristics of PW30

After determining current-voltage and power-voltage characteristics from an indoor solar simulator, the pair of glass coated PV modules was installed in the test section of an outdoor room. The outdoor experiments were conducted on PV modules in order to determine electrical and thermal characteristics and further improving the overall performance of PV modules by using thermal mass of an outdoor room.

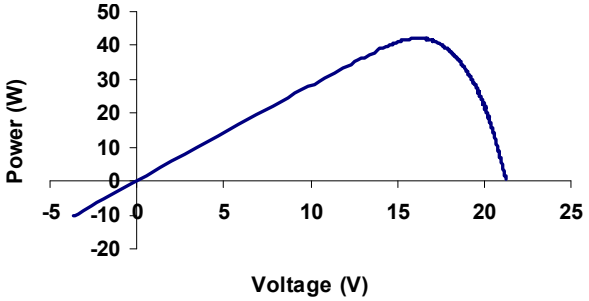

Fig. 4 Power-voltage characteristics of PW30

III. OUTDOOR EXPERIMENTS

The outdoor room was a pre-fabricated structure that was delivered into the premises of Concordia University in Montréal, Québec, Canada for conducting experiments on glass coated PV modules [1]. The test section with vertical PV modules, was aligned 10° East of South for receiving maximum solar radiation between 8.00 and 14.00 hrs solar time and also avoiding shading from adjacent buildings [1]. The schematic of an outdoor room used for conducting outdoor experiments is illustrated in Fig. 5 [1]. The outdoor experiments were conducted on a solar wall section built with two commercially available glass coated PV modules, an air passage with gap width of 90 mm, an insulating panel, side walls made up of plexiglas and connected wooden frames [1]. The insulation panel was assembled with 7 mm thick plywood board enclosure filled with 26 mm polystyrene [1]. The steady state average resistance of the composite plywood board-polystyrene section of insulation panel obtained from the heat flow meter test was 1.0 m^2 °C W^{-1} [1]. The side wall of wooden frame was fixed with plexiglas of thickness 12 mm (k = 0.1316 W m^{-1} K^{-1}) placed perpendicularly facing air-gap for view of the air passage from inside the test room.

A series electrical circuit connection was established for a pair of vertical PV modules installed on a solar wall for determining the current-voltage measurements and electric power output. The electrical circuit for two PV modules connected in series for generation of electric power with a rheostat of maximum varying resistance up to 50 Ω is illustrated in Fig. 6 [1]. A circular variable resistor of 50 Ω was a wire-wound coil with a sliding contact that was used to vary electrical resistance without interrupting the current. The Joule heating at a rate of 73 cal/s (305 W) was predictable at a typical current rating of 2.8 A for a PV module. The null resistance of rheostat was calculated to be 39 Ω at a current of 2.8 A, which was not having any potential difference across it. In Fig. 6, the sliding contact of rheostat has a resistance of R_s, with a current ($i = V_r/R_s$) flowing across the circuit; V_r is potential difference across the resistance, R_s.

The passive air ventilation was created in the PV module test section by natural wind or through buoyancy effect in the absence of wind [1]. The active fan pressure was used to achieve higher air velocities by operation of the exhaust fan fixed on opposite façade with respect to the PV test section [1]. The slight negative pressure was induced for drawing low air velocities in absence of wind-induced pressure from the

inlet damper into the PV test section through the outdoor room [1]. The exhaust ventilation fan was rated at 270 CFM (ft3/min) (0.127 m^3 s^{-1}) at standard atmospheric pressure so as to create between 10-25 Pa of negative pressure depending on the air leakage from the outdoor room [1].

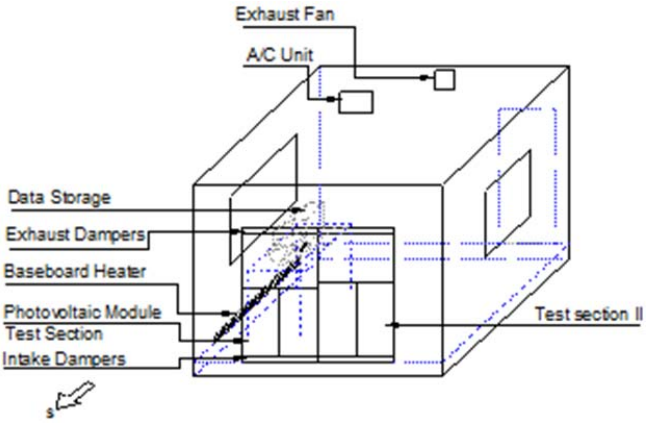

Fig. 5 Schematic of a pre-fabricated outdoor room with PV solar wall test section

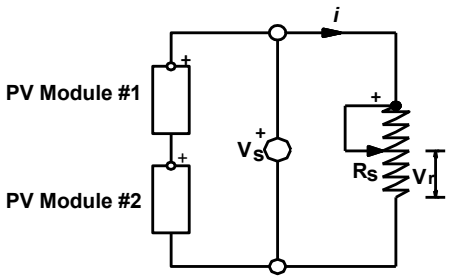

Fig. 6 Electric circuit for PV modules

The air velocities near the exit of PV modules were obtained both as a measure of buoyancy and fan induced hybrid ventilation. The fan pressure was created with an exhaust fan fixed on wall of an outdoor room opposite to wall with a wooden frame installed with glass coated PV modules. The air velocity sensor was placed perpendicular to the walls of the PV solar wall section for measuring axial air velocities near its outlet [1].

In order to minimise boundary layer effect in air velocity measurement, air velocity sensor was placed at middle air-gap width at a distance of 45 mm from either of the walls of the PV solar wall [1]. To minimise turbulence effects in air velocity measurement, air velocity sensor was placed near the outlet (at 1100 mm from the bottom) of the PV test section with total air passage length of 2100 mm in the test section. To minimise three-dimensional effect in air velocities, fan-induced active ventilation was achieved by developing air velocities by the induced draft fan fixed on the opposite wall so that it was placed at a distance from the walls of PV module test section [1]. It was validated by one of the experiments that measured surface temperatures of the two adjacent glass coated PV modules were within ±0.5 °C under similar operating conditions [1].

A. Instrumentation

The voltage and current outputs from the transducers placed on different positions on the experimental apparatus were connected to the Agilent 34970A data acquisition system. VEE Pro software is used to design and build control functions for collection and storage of the measurement data. The collected data in the data logger were imported to the computer in Notepad and Microsoft Excel programs with use of VEE Pro software. The Agilent 34970A data acquisition system was calibrated with a multi-meter by comparison of output signals from the sample measurements. The measurements collected in the data logger were up to six significant figures [1].

The copper-constantan junction (T-type) thermocouples were used for measurements for generating voltage signals to the data logger. All the thermocouples connected to the data acquisition system were machine cut and manually made from single roll of wire. The thermocouples were calibrated using heat flow meter (model: Dynatech R-Matic). The instrument was used to measure surface-to-surface resistance of test samples with thickness up to 200 mm as per ASTM C-518 (ASTM Standard, 1985). In order to calibrate thermocouple wires, one differential thermocouple was made from the roll of thermocouple wires and was fixed on the wooden test sample (with known RSI value) which was placed inside the calibrated heat flow meter to generate the voltage output signal. The signal generated was compared with the output given by the heat flow meter. Based on comparison of measurements, uncertainty or inaccuracy in obtaining measurements using thermocouple sensors was estimated at ± 0.05 °C. Sensors of thermocouples used to measure air temperature were either exposed to solar or surface radiations and therefore were shielded (without contact with sensors) by right angled cones made of opaque tape covered with aluminium reflective coating to avoid radiation effect in temperature measurements. Dimensions of a typical cone were: base radius of 10.0 mm and height of 30.0 mm. For thermocouples used to measure surface temperatures, aluminium coated tape exposed to solar radiation was fixed on the surface area in contact with the sensor to avoid error in measurement due to radiation. It was assumed that sensible heat storage capacity of aluminium coated tape used to shield sensors of thermocouples was nil in comparison with that of thermocouple wires made of copper-constantan junction.

The operation of air velocity sensor (make-Dwyer instruments, model no. 640-0) was based on the current output and has four field selectable ranges for air velocity measurement from 0 to 60 m/s and has accuracy of ±5% of full scale reading in the range of 0-1 m/s at the operating air temperature range of 0-100 °C. In order to minimise boundary layer effect in air velocity measurement, air velocity sensor was placed at middle air-gap width at a distance of 45 mm from either of the walls of the solar wall. To minimise turbulence effects in air velocity measurement at the entrance and exit region of the solar wall, velocity sensor was placed near the outlet (at 1100 mm from the bottom) of the PV solar wall with total air passage length of 2100 mm in the test

section.

The solar intensity measurements were performed with the photometer sensor fixed on the building façade of an outdoor room with installed PV solar wall. The calibration of the photometer was performed with the calibrated pyranometer of known correction factor. The output signals from the photometer and pyranometer were compared (at known solar intensity) with a multi-meter, and correction factor for the photometer was obtained. The measurement sensor in the photometer was based on a silicon solar cell. It was assumed that the radiation characteristics of the PV module and photometer were in the same radiation spectrum, thus minimising the measurement error induced due to incident angle dependency of surface radiation properties. Other reasons for using the photometer for measurement of the solar intensity were its light weight, easiness, and robustness in fixing on building façade in comparison with the similar practical setup performed with a heavy as well as delicate pyranometer.

B. Outdoor Measurements

Three thermocouple sensors were placed at the top, middle, and bottom locations in the PV module, air-passage, and insulating panel. They were used to measure their local temperatures at their defined fixed positions [1]. Two thermocouples were used to measure the inside test room air temperature and ambient air temperature [1]. One differential thermocouple was used to check the air temperature difference between top and bottom sections of the PV module test section [1]. The thermocouple outputs, current, voltage, solar irradiation, and air velocity signals were connected to a data logger and a computer for data storage [1]. The copper-constantan junction (T-type) thermocouples were used for measurements for generating voltage signals to the data logger [1]. As mentioned earlier, the air velocity sensor (make-Dwyer instruments, model no. 640-0) was used to collect air velocity measurements. The solar intensity measurements were collected with a photometer sensor fixed on the south wall of an outdoor room.

C. Temperature Plots

The measurements collected from the sensors were recorded in a data logger as a function of air velocities through a PV solar wall for the cases of passive ventilation and active ventilation with use of fan pressure. Similarly, temperature measurements were obtained from the PV solar wall section as a function of air velocities. The temperatures for PV module, air passage, and insulating panel in the PV solar wall were obtained. The sample measurements obtained from outdoor experimental setup are presented in Table II.

The temperature plots for PV module, insulating panel, and air for different conditions of ventilation are illustrated in Figs. 8 and 9. The temperature plots with respect to height of a PV solar wall for the data provided in Tables II to IV are obtained. The variation of mean temperatures of PV module, insulating panel, and air in a PV solar wall with approximately steady solar noon irradiation with varying air velocities for the case of active ventilation and passive ventilation are illustrated in Figs. 10-12.

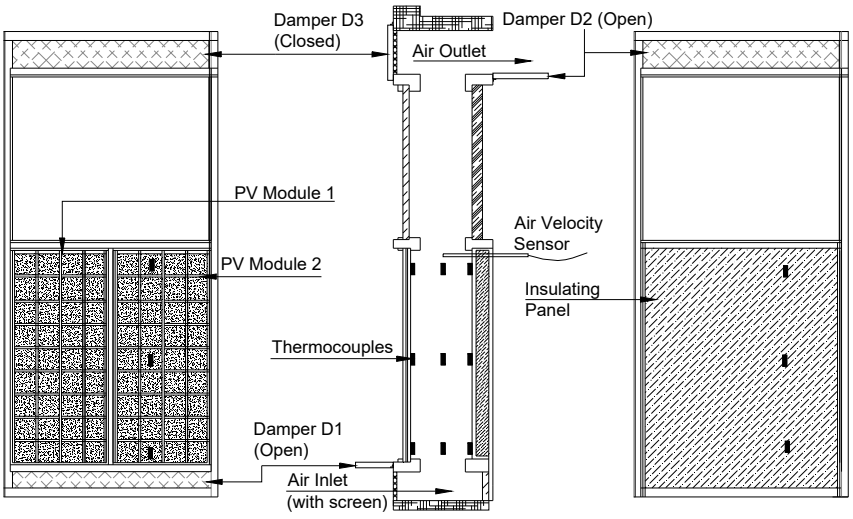

Fig. 7 Schematic of outdoor experimental apparatus for a PV solar wall installed on a wooden frame

D. Sensible Heat Storage Capacity

The PV solar wall test section with wooden frame was composed of non-homogeneous materials having different densities, specific heats, and thicknesses. The pair of PV modules was fixed with three layers of material, viz. a flat sheet of solar cells, glass sheets on its exterior and interior sides. It was assumed that surface temperature of PV module was uniformly distributed in the three layers. It was also assumed that the heat capacity of the wooden frame and sealing material was having little effect on the temperature of PV module, air or insulation panel. This was because of the fact that wood was used as a construction material, and moreover, the magnitude of the heat capacity of wood framing material was not proportional to the face area of glass coated PV modules. The sensible heat capacities of glass faces, solar

cells, air and polystyrene filled plywood board are presented in Table III. It was observed that the difference of temperatures recorded by the top and bottom sensors for PV module, air and insulating panel were 6.9 °C, 8.1 °C, and 9.9 °C, respectively, for the critical case of passive ventilation of Run no. 4 in Table II. Furthermore, the temperature differences were used for obtaining sensible heat storage capacities of various components in y-ordinate. The heat storage capacities obtained were 59.6 kJ, 0.755 kJ, and 510.7 kJ for PV module, air and insulation panel respectively. The heat capacities obtained were negligible in comparison with the total daily solar irradiation on PV modules on the day of conducting the outdoor experiments. It was also assumed that there were constant surface properties and ideal still air at the instance of collection of the measurements. Heat storage capacity in x-ordinate was also obtained from the similar procedure by assuming same proportionate temperature difference along thicknesses in x-ordinate. It was found that heat capacity in x-ordinate was nil in comparison with the value of heat capacity obtained for y-ordinate.

TABLE II
OUTDOOR MEASUREMENTS

Run No.	S (W m^{-2})	E_p (W)	T_o (°C)	T_s (°C)	V (m s^{-1})
Active ventilation (Fan-induced)					
1	716.1	30.7	15.2	22.4	0.68
2	716.1	30.7	13.4	22.4	0.53
Passive ventilation (Buoyancy-induced)					
3	697.5	28.9	13.2	25.1	0.13
4	697.5	28.8	13.3	24.9	0.17

Run No.	T_p(b) (°C)	T_p(m) (°C)	T_p(t) (°C)	T_b(b) (°C)	T_b(m) (°C)	T_b(t) (°C)	T_a(b) (°C)	T_a(m) (°C)	T_a(t) (°C)
Active ventilation (Fan-induced)									
1	35.4	33.8	36.8	20.6	24.7	29.1	18.8	21.7	19.4
2	35.9	34.6	37.9	20.9	25.0	29.5	19.3	22.5	19.9
Passive ventilation (Buoyancy-induced)									
3	40.8	44.9	46.8	27.9	34.8	38.0	21.3	29.5	29.8
4	39.9	45.0	46.8	28.4	35.0	38.3	21.7	28.3	29.8

Distance as per locations shown in Fig. 7	T_p(b) (°C)	T_p(m) (°C)	T_p(t) (°C)	T_b(b) (°C)	T_b(m) (°C)
y (cm)	15	55	94	15	55
z (cm)	60	60	60	60	60
x (mm)	6.2	6.2	6.2	96.2	96.2

Distance as per locations shown in Fig. 7	T_b(t) (°C)	T_a(b) (°C)	T_a(m) (°C)	T_a(t) (°C)	Air velocity sensor
y (cm)	94	15	55	94	99
z (cm)	60	60	60	60	60
x (mm)	96.2	51.2	51.2	51.2	51.2

Note: x is horizontal; y is vertical; z is adjacent 3rd axis of x-y plane

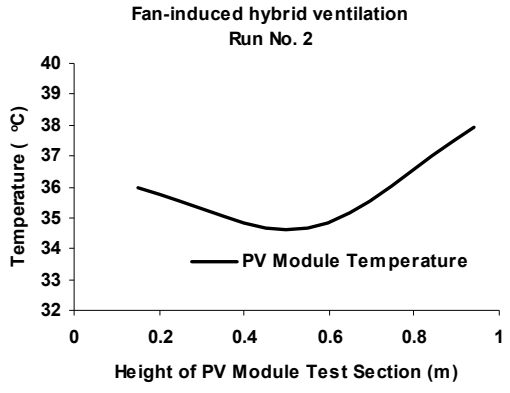

Fig. 8 (a) Temperature plot of PV module for fan-induced hybrid ventilation with height of PV solar wall section

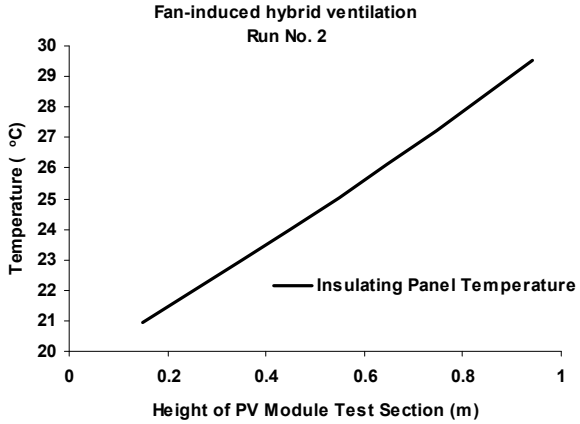

Fig. 8 (b) Temperature plot of insulating panel for fan-induced hybrid ventilation with height of PV solar wall section

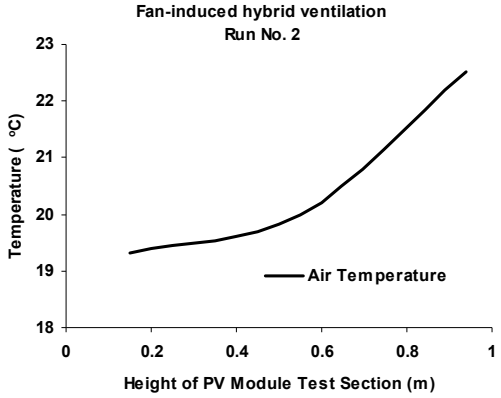

Fig. 8 (c) Temperature plot of air for fan-induced hybrid ventilation with height of PV solar wall section

TABLE III
SENSIBLE HEAT STORAGE CAPACITIES

Component	ρ_n (kg m^{-3})	C_n (J kg^{-1} K^{-1})	d_n (m) X 10^{-3}	$d_n\rho_nC_n$ (J m^{-2}K^{-1})	$H_{pv\text{-}T}$ (J K^{-1})
Glass coating	3000	500	3	4500	4171.5
PV module	2330	677	0.2	315.48	292.45
Glass coating	3000	500	3	4500	4171.5
Sub-total	-	-	-	-	8635.5
Air	1.1174	1000	90	100.56	93.22
Plywood	550	1750	7	6737.5	6245.66
Polystyrene	1050	1200	26	32760	30368.5
Plywood	550	1750	7	6737.5	6245.66
Sub-total	-	-	-	-	42953.0
Total	-	-	-	-	51588.5

Note: Heat capacities were calculated for face area of PV module test section of 0.927 m^2.

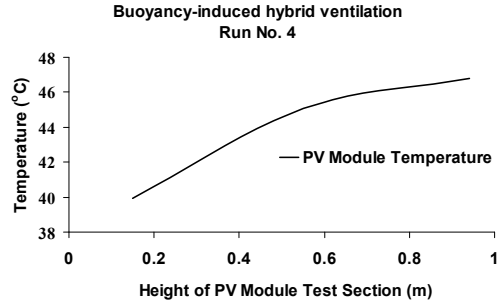

Fig. 9 (a) Temperature plot of PV module for buoyancy-induced hybrid ventilation with height of PV solar wall section

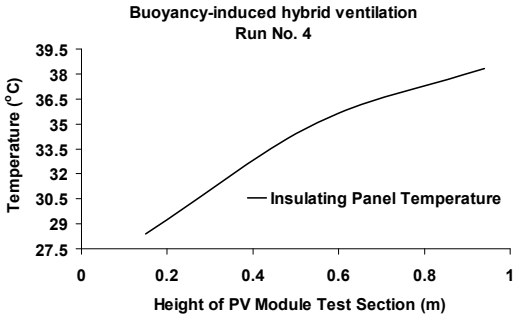

Fig. 9 (b) Temperature plot of insulating panel for buoyancy-induced hybrid ventilation with height of PV solar wall section

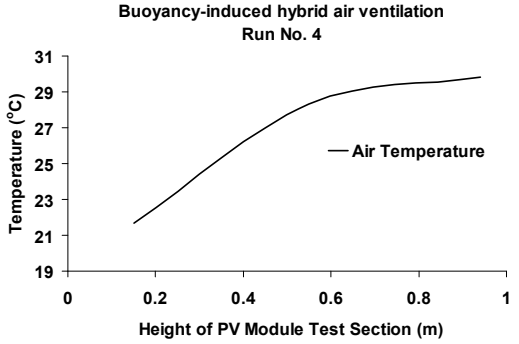

Fig. 9 (c) Temperature plot of air for buoyancy-induced hybrid ventilation with height of PV solar wall section

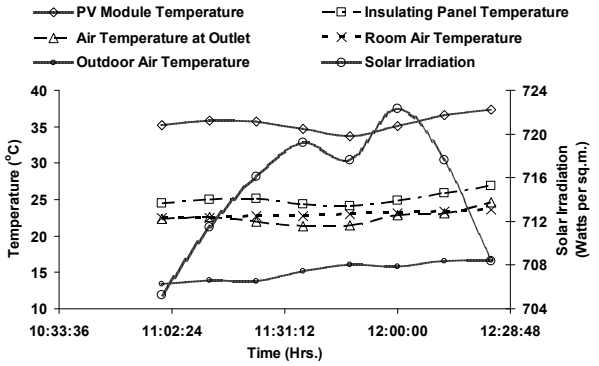

Fig. 10 Variation of mean temperatures of PV module, air and insulating panel with solar irradiation under fan-induced hybrid ventilation

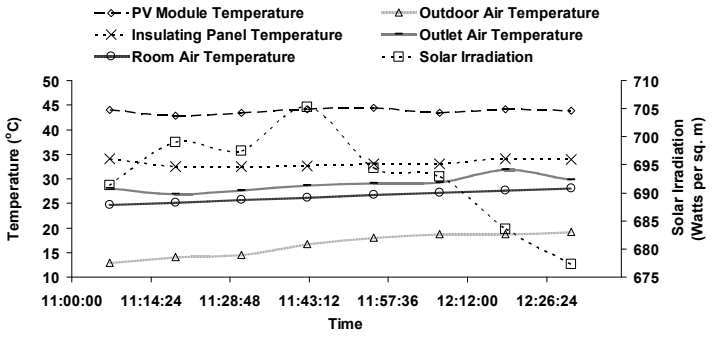

Fig. 11 (a) Variation of mean temperatures of PV module, air and insulating panel with solar irradiation under buoyancy-induced hybrid ventilation

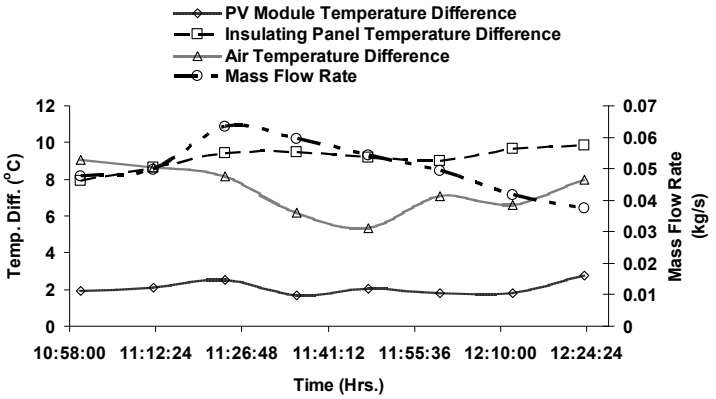

Fig. 11(b) Temperature difference for PV module, insulating panel and air with height of PV solar wall under fan-induced hybrid ventilation

TABLE IV
THERMAL STORAGE CAPACITIES

Component	k_d (W m^{-1} K^{-1})	$d_n\rho_nC_n$ (J m^{-2}K^{-1})	H_d (Wm^{-2}K^{-1})	T (sec)	ΔT_V (K)	ΔT_H (K)	Q_V (kJ)	Q_H (J)
PV module	0.91	9315.48	10	932	6.9	0.04	5.8	0.2
Air	0.02624	100.56	10.0	10	8.1	0.75	0.0	0.0
Plywood	0.0835	6737.5	10.0	674	9.9	0.40	0.55	0.16
Polystyrene	0.02821	32760	1.0	32760	9.9	0.40	9.0	9.6
Plywood	0.0835	6737.5	10.0	674	9.9	0.40	0.55	0.16
Total	-	-	-	-	-	-	15.9	10.12

Notes:
1. Equivalent thermal conductivity of glass coated PV module was calculated to be 0.91 W m^{-1} K^{-1}
2. Temperature differences along y-direction i.e. along height of PV module test section (0.993 m) were obtained from Table III for Run No. 4 in the case of buoyancy-induced hybrid ventilation.
3. Temperature differences along x-direction i.e. along thicknesses of each component of PV module test section were obtained proportionate to temperature differences along y-direction.

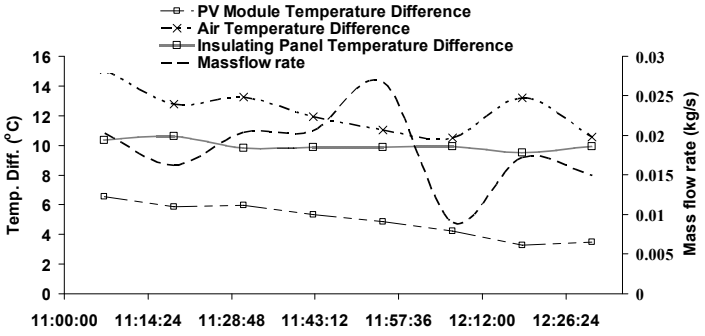

Fig. 12 Temperature difference for PV module, insulating panel and air with height of PV solar wall under buoyancy-induced hybrid ventilation

E. Thermal Time Constant

The thermal time constant is defined as the time required for the outlet air temperature to attain 63.2% of the total difference in value attained in air temperature following a step change in temperature of outdoor air crossing the inlet opening of the PV solar wall. Data for a step change were selected for observing the ambient air temperature. The data selected were in a steady state before and after the time-interval during the unsteady state response of the outlet air temperature with the step change in ambient air temperature. From the graphs, it was observed that thermal time constant under passive air ventilation was between 8-10 minutes in comparison to 2 minutes under active air ventilation. Therefore, it was decided that duration of time interval was selected for a minimum of two minutes to record any subtle temperature changes for obtaining measurements from the data logger [1]. The graphs of ambient and outlet air temperatures were plotted against the time-interval of measured data for the two cases of passive and active ventilation are presented in Fig. 13(a) and (13(b).

Thermal time constants of the PV solar wall section were function of ambient air temperatures and air velocities and were therefore approximately calculated under conditions of passive and active air ventilation.

IV. DISCUSSIONS

The electrical characteristics that were obtained for a pair of

glass coated PV modules with indoor experiments under standard operating conditions were performed under ideal conditions. The ideal test conditions gave inconclusive characteristics which certainly are not suitable for consideration during design of PV module system connected to buildings. Additional information under available operating conditions was essential for system design of the PV module system.

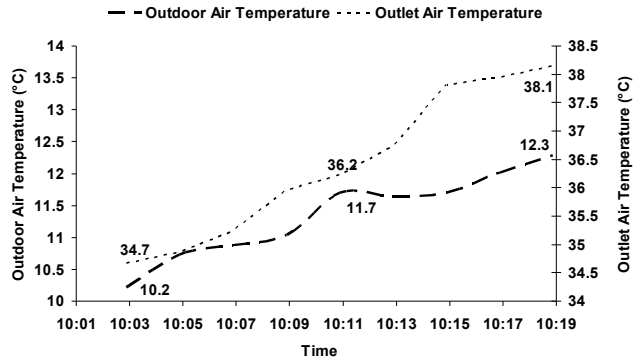

Fig. 13 (a) Changes in outlet air temperature from a PV solar wall with a step change in outdoor air temperature under passive (buoyancy-induced) ventilation

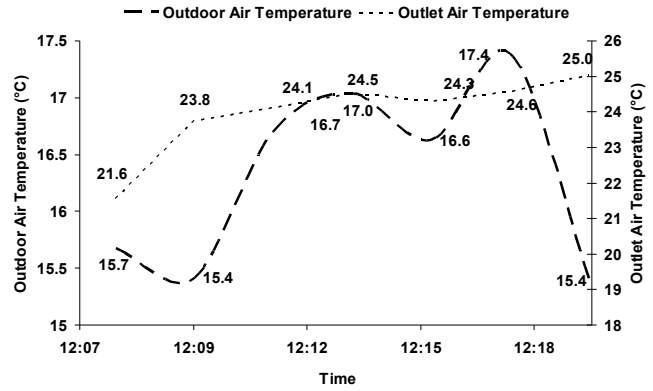

Fig. 13 (b) Changes in outlet air temperature from a PV solar wall with a step change in outdoor air temperature under active (fan-induced) ventilation

The results of outdoor experiments revealed that thermal characteristics of PV modules were improved with a glass coating. There was considerable loss in generation of electrical power from a pair of glass coated PV module in comparison to typical rated electrical power for a PV module. The glass coating was responsible for increasing thermal storage along the major dimensions of the PV module system. The conduction heat flow along the height of the glass coated PV module resulted in rise of temperature along its height. This resulted in formation of thermal gradients along the volume of PV module system. The original metallic frame of the glass coated PV module was replaced with a wooden frame to minimise the effect of thermal gradients.

The insulating panel in the wooden frame was a plywood board filled with polystyrene which is used in a modern building for insulation. The temperature plots of Figs. 8 and 9 show that there was steep rise in temperature of insulating panel in comparison to glass coated PV module. The air temperature of air passage in the PV module test section was increased considerably due to increase in thermal mass of the PV module system connected to a building. A comparison of experimental results of passive and active ventilation envisaged that active ventilation was necessary to reduce high temperatures of PV modules. The heat storage capacities and thermal storage capacities of various components of PV module system were calculated. The major heat storage in the PV module system was due to heat capacities of the insulating panel. The result was loss of heat along the height of the PV module system. The packed polystyrene with loose fills in the plywood board was responsible for increasing thermal storage capacity of insulating panel. The rise in temperature along the thickness was calculated proportionally from the observed temperature rise along the height of the PV module system. Hence, the temperature measurements were also obtained along the volume, viz. height of a PV solar wall system as per sensor locations depicted in Table II.

V. Conclusion

A PV solar wall was investigated by means of indoor and outdoor experiments. The outdoor experiments were conducted on a PV solar wall installed on a wooden frame connected to a room with passive and active ventilation. Further, outdoor experiments were established under available operating conditions. The experiments conducted on a PV solar wall have taken into consideration the effect of heat capacity, thermal time constant, and thermal storage losses. The electrical and thermal characteristics were established for a PV solar wall. The sensible heat storage capacities of a PV solar wall installed on a wooden frame were higher in comparison to a window glass or a stand-alone PV module. The electrical and thermal characteristics were function of both outdoor air temperature and thermal storage losses. Finally, production of heat and electricity was a nonlinear function of volume of electrical and thermal resistances developed across a PV solar wall. The active ventilation was deemed to be essential in order to avoid over-heating of a PV solar wall and to maintain adequate outdoor ventilation in a room under mild climate conditions.

Nomenclature

Tp	Temperature of PV module
Tb	Temperature of insulating panel
Ta	Temperature of air
S	Solar Intensity
Ep	Electric power
V	Air velocity
To	Ambient air temperature
Ts	Room air temperature
Hpv-	T Heat capacity
ΔTv	Temperature difference (y-ordinate)
ΔTH	Temperature difference (x-ordinate)
ρn	Density
Kd	Thermal conductivity

Hd	Film coefficients
T	Thermal time constant
Qv	Thermal storage capacity (y-ordinate)
QH	Thermal storage capacity (x-ordinate)
Cn	Specific heat
dn	Thickness
dnρnCn	Energy stored/m2/K
Isc	Short circuit current
Voc	Open circuit voltage

ACKNOWLEDGMENT

Part of the work was conducted by the author at Department of Building, Civil and Environmental Engineering, Concordia University, Montréal, Québec, Canada.

REFERENCES

[1] H. Dehra, "A numerical and experimental study for generation of electric and thermal power with photovoltaic modules embedded in building façade," submitted/un-published Ph.D. dissertation, Dept. Building, Civil and Environmental Engineering, Concordia University, Montréal, Québec, Canada. August 2004.

[2] H. Dehra, "Experiments on photovoltaic modules embedded in building façade," AIChE Spring 2010, San Antonio, TX, USA, March 21-25, 2010.

[3] H. Dehra, "A combined solar photovoltaic distributed energy source appliance," Natural Resources, pp. 75-86, Issue 2, 2011.

[4] H. Dehra, "The effect of heat and thermal storage capacities of photovoltaic duct wall on co-generation of electric and thermal Power," AIChE 2007 Spring Meeting, Houston, Texas, USA, April 22-26, 2007, session 36a.

[5] C. Muresan, C. Ménézo, R. Bennacer, R. Vaillon, "Numerical simulation of a vertical solar collector integrated in a building frame: radiation and turbulent natural convection coupling," Heat Transf Eng, pp. 29-42, 27, 2006.

[6] J. H. Kim, J. T. Kim, "A simulation study of air-type building-integrated photovoltaic-thermal system," Energy Procedia, pp. 1016-1024, 30, 2012.

[7] Y. Lin, C. Chiang, C. Lai, "Energy efficiency and ventilation performance of ventilated BIPV walls," Eng Appl Comput Fluid Mech, pp. 479-486, 5, 2011.

[8] C. J. Ho, A. O. Tanuwijava, C. Lai, "Thermal and electrical performance of a BIPV integrated with a micro encapsulated phase change material layer," Energy Build, pp. 331-338, 50, 2012.